Duct Shape Design Technology Based on Evolutionary Algorithm Considering Noise Attenuation Performance and Air Permeability

Satoshi TABUCHI*1

*1 AI Promotion Project Department, Technical Development Group

This paper relates to a technique for designing the engine room of a hydraulic excavator equipped with an Integrated Noise & Dust Reduction (iNDr) cooling system. In order to improve the noise attenuation performance, changes in cross-sectional area and bends have been introduced into the muffler duct of the iNDr structure. On the other hand, changes in cross-sectional area and bending will deteriorate the air permeability and decrease the cooling capacity. Thus, in a muffler duct, the air permeability of the cooling air and noise attenuation performance are in a trade-off relationship. Against this backdrop, an optimum design technology has been developed using a multi-objective genetic algorithm (MOGA) to achieve both air permeability and noise attenuation performance in the intake duct of the iNDr structure of the engine room. This technology has enabled the design of an engine-room shape taking both the air permeability and noise attenuation performance into account.

Introduction

Construction in urban areas and during nighttime is increasing, and there is an increasing demand for reducing the noise of construction machinery, considering the environment around work sites and improving the working environment for operators. Kobelco Construction Machinery Co., Ltd. developed an Integrated Noise & Dust Reduction Cooling System (iNDr) to reduce the noise level (**Fig. 1**).[1] The iNDr has improved the soundproofing performance by closing gaps in the engine room and employing an offset duct structure, in which the inlet and outlet openings for cooling air are disposed only on the upper surface of the machine body. As a result, the hearing ability of workers in the vicinity is secured, thus improving their safety, and noise in work site neighborhoods has been improved.

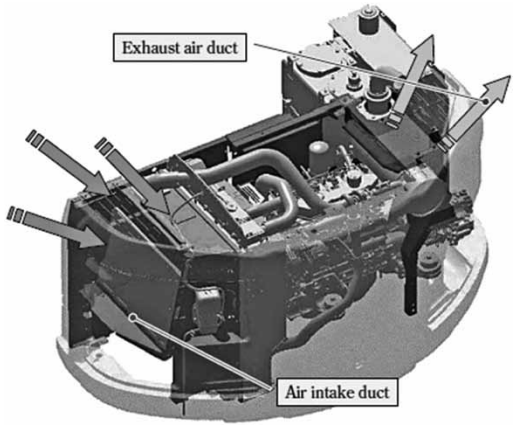

Fig. 1 Structure of iNDr[1]

In the meantime, the strengthening of emissions regulations in recent years has been causing changes in the design of cooling systems to cope with the increasing amount of heat generated in engines, as well as changes in the layout of the machine bodies due to the addition of exhaust purification devices.

In the case of the iNDr, any change in the layout of the machine body requires its duct shape to be determined so as to minimize the leakage of sound from the opening of its offset duct and, at the same time, to secure the amount of cooling air necessary for establishing the heat balance; it is difficult to solve these issues simultaneously. So far, the structure of the iNDr duct has been determined by repeated examinations with numerical analysis and bench testing, posing a challenge to shortening the development period.

It was against this backdrop that a technique using an evolutionary algorithm (hereinafter referred to as "EA")[2] was developed to design a duct taking both the ventilation resistance and noise attenuation performance into account. This paper introduces an example applied to the designing of the iNDr intake duct.

1. Optimization of duct shape using evolutionary algorithm

1.1 Optimization technique

The design of an intake duct must take both the ventilation resistance and noise attenuation into account, posing a problem of two-objective optimization with the objective functions of ventilation resistance and noise attenuation. In this paper, a multi-objective optimization technique is used to pursue the right duct shape for achieving both low resistance and low noise. The duct shape has been optimized by the genetic algorithm (hereinafter referred to as "GA") that is considered to be the most common among the EAs for multi-

objective optimization.

1.2 Genetic algorithm

A GA is an optimization technique inspired by the evolutionary process of living organisms and has the capability of being adapted for complicated objective functions. It is often used when there are many design variables. This is owing to the global solution searching capability of GAs even for multimodal objective functions.

Fig. 2 shows the solution procedure using a genetic algorithm. The GA consists of the process steps of Initialization generating multiple individuals, followed by Selection, Crossover, Mutation, and Evaluation of the individuals.

In Initialization, a range of possible values for each design parameter is preset, and a plurality of design solution candidates composed of a combination of a plurality of design parameters is generated using random numbers. In Evaluation, the performance of each design solution candidate generated is digitalized and evaluated, and excellent design solutions with high evaluation values are chosen in Selection.

In Crossover, two design solutions are selected from the plurality of design solutions generated, and one with a combination of design parameters similar to those two design solutions is newly generated. Mutation is an operation that changes, at a certain probability, some parts of the parameters of the design solution with random numbers so as to create new combinations of design parameters. This operation guarantees the diversity of the solutions and prevents them from being mere local optimal solutions.

While the steps of Selection, Crossover, Mutation, and Evaluation are being repeated, the features combining excellent design parameters are inherited during the search for new solutions, enabling the search for a solution with the highest evaluation value of the target performance. In actual design, it is important to obtain solutions in a short time. Because GA repeatedly performs the creation and evaluation of design solutions, an evaluation method with a high calculation load is not suitable for the evaluation of performance. Hence, an approximate expression of the objective function with variables of the design parameters was constructed from the results of the numerical analysis of a small number of simple shapes and was used for the evaluation. This made it possible to significantly shorten the time, compared with using numerical analysis for the evaluation of the objective function.

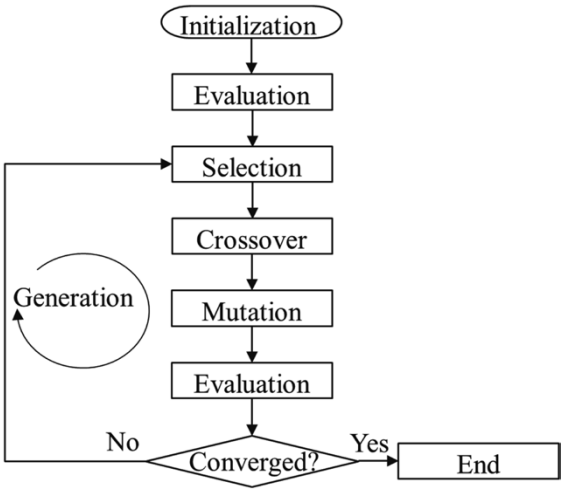

Fig. 2 Procedure for solving by genetic algorithm

2. Application to designing of intake duct

2.1 Duct shape

Fig. 3(a) is the schematic diagram of an intake duct for an iNDr system. This iNDr intake duct is simplified to produce the model shown in Fig. 3(b). The following is a consideration of the optimization of the simplified duct shape in Fig. 3(b). The intake duct of an iNDr is configured to take in the outside air from a rectangular opening on the top while the fan installed in the circular opening in the lateral face is in operation. Now, the duct is divided into two parts (**Fig. 4**(a)-(c)), and ventilation resistance and noise attenuation performance are evaluated for each of the duct parts. Here, the part shown in Fig. 4(b) is referred to as Duct A, and the part shown in Fig. 4(c) is referred to as Duct B. The outer shape of the duct was regarded as being defined by fixed values, since it is affected by the size of the machine body. As shown in Fig. 4, the design variables were set to be the ten dimensions defining the opening area and the opening position of the intake duct.

2.2 Mathematical modeling of ventilation resistance

The prediction equation for pressure loss in an

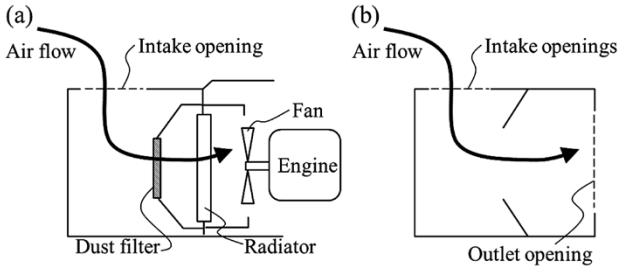

Fig. 3 Schematic image of intake duct
(a) iNDr system (b) simplified model

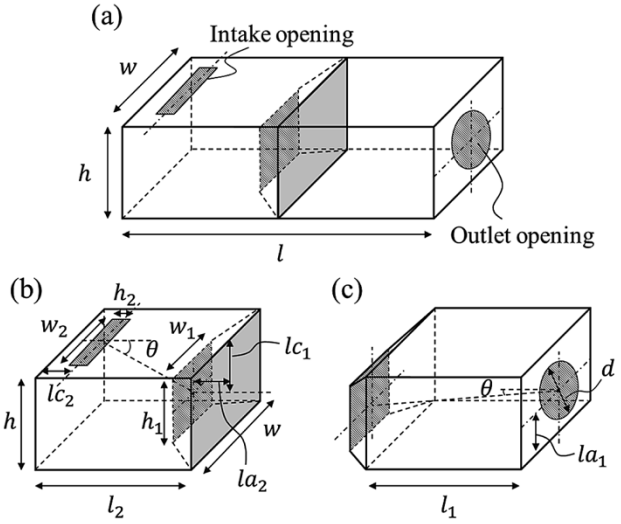

Fig. 4 Design variables for intake duct
(a) whole model (b) Duct A (c) Duct B

expansion-type silencer is proposed by Yoshihara,[3] and the prediction equation for pressure loss in an S-type silencer like Duct A is given by Equation (1). Shapes like that of Duct B are classified into Q-type and P-type depending on the presence or absence of an eccentric angle, and their pressure losses are expressed by Equations (2) and (3), respectively:

$$\Delta P = 1.808 m_A^{\frac{1}{8}} n_A^{\frac{1}{12}} \frac{\rho v^2}{2} \quad \cdots\cdots (1)$$

$$\Delta P = 0.324 m_B^{\frac{1}{8}} n_B^{\frac{3}{4}} \frac{\rho v^2}{2} (\text{for } \theta = 0) \quad \cdots\cdots (2)$$

$$\Delta P = 2.021 m_B^{\frac{1}{8}} n_B^{\frac{1}{12}} (\tan\theta)^{\frac{1}{8}} \frac{\rho v^2}{2} (\text{for } \theta \neq 0) \quad \cdots\cdots (3)$$

wherein,

ΔP: pressure loss of the duct
m_A (=S_C / S_A): expansion ratio of Duct A
m_B (=S_C / S_B): expansion ratio of Duct B
S_A (=$h_2 w_2$): opening area on the inflow side of Duct A
S_B (=$h_1 w_1$): opening area on the inflow side of Duct B
S_C (=h_w): cross-sectional area of the duct
n_A (=l_2 / d_A): cavity length ratio of Duct A
n_B (=l_1 / d_B): cavity length ratio of Duct B
d_A : hydraulic equivalent diameter of the opening on the inlet side of Duct A
d_B : hydraulic equivalent diameter of the opening on the inlet side of Duct B
θ : eccentric angle
ρ : air density
v : average flow velocity on inflow side

Yoshihara's equation is an estimation equation based on the experimental results for an inlet with a fixed inner diameter. Hence, in order to make the inlet shape serve as a shape design parameter, it is necessary to newly construct a prediction expression that takes into account the influence of the inlet shape.

For the mathematical modeling of ventilation resistance described in this paper, computational fluid dynamics (hereinafter referred to as "CFD") was used to calculate the pressure loss values of multiple ducts to construct experimental equations expressing the relationship among the dimensions of the duct and its pressure loss.

The duct subjected to shape optimization this time has 10 dimensions as its design parameters. In order to suppress the number of cases to be analyzed, the design parameters were selected using L18 orthogonal arrays so that the combination of design parameters greatly varies from case to case. Eighteen cases of analysis conditions were set on the basis of the L18 orthogonal arrays, and 18 types of numerical analyses were performed in each case to construct experimental equations from the results obtained by the numerical analyses. **Table 1** and **Table 2** respectively show the design parameters of Duct A and Duct B subjected to CFD. **Fig. 5** shows an example of the computational meshes used for the analysis.

Fig. 6 shows the factor effect diagram for Duct A, while **Fig. 7** shows the same for Duct B. As shown in Fig. 6, the pressure loss value of Duct A decreases with increasing opening width w_1 and opening height h_1 on the outflow side. It is found that the pressure loss is particularly sensitive to the change of the opening width w_1 on the outflow side. Fig. 7 shows that the pressure loss decreases as the diameter d of the opening on the outflow side increases. Yoshihara's equation does not include the

Table 1 L18 orthogonal arrays for Duct A

Case	l_2	la_2	lc_1	lc_2	h_1	h_2	w_1	w_2
1	0.60	0.10	0.35	0.20	0.40	0.25	0.30	0.30
2	0.60	0.10	0.40	0.25	0.50	0.30	0.50	0.50
3	0.60	0.10	0.45	0.30	0.60	0.35	0.70	0.70
4	0.80	0.10	0.45	0.25	0.60	0.25	0.50	0.30
5	0.80	0.10	0.35	0.30	0.40	0.30	0.70	0.50
6	0.80	0.10	0.40	0.20	0.50	0.35	0.30	0.70
7	1.00	0.10	0.45	0.20	0.50	0.30	0.70	0.30
8	1.00	0.10	0.35	0.25	0.60	0.35	0.30	0.50
9	1.00	0.10	0.40	0.30	0.40	0.25	0.50	0.70
10	0.60	0.20	0.35	0.30	0.50	0.35	0.50	0.30
11	0.60	0.20	0.40	0.20	0.60	0.25	0.70	0.50
12	0.60	0.20	0.45	0.25	0.40	0.30	0.30	0.70
13	0.80	0.20	0.40	0.30	0.60	0.30	0.30	0.30
14	0.80	0.20	0.45	0.20	0.40	0.35	0.50	0.50
15	0.80	0.20	0.35	0.25	0.50	0.25	0.70	0.70
16	1.00	0.20	0.40	0.25	0.40	0.35	0.70	0.30
17	1.00	0.20	0.45	0.30	0.50	0.25	0.30	0.50
18	1.00	0.20	0.35	0.20	0.60	0.30	0.50	0.70

Table 2 L18 orthogonal arrays for Duct B

Case	l_1	la_1	la_2	lc_1	h_1	w_1	d
1	0.30	0.55	0.10	0.35	0.40	0.30	0.40
2	0.30	0.45	0.20	0.40	0.50	0.50	0.50
3	0.30	0.35	0.30	0.45	0.60	0.70	0.60
4	0.40	0.45	0.10	0.45	0.60	0.50	0.40
5	0.40	0.35	0.20	0.35	0.40	0.70	0.50
6	0.40	0.55	0.30	0.40	0.50	0.30	0.60
7	0.50	0.55	0.10	0.45	0.50	0.70	0.50
8	0.50	0.45	0.20	0.35	0.60	0.30	0.60
9	0.50	0.35	0.30	0.40	0.40	0.50	0.40
10	0.60	0.35	0.10	0.35	0.50	0.50	0.60
11	0.60	0.55	0.20	0.40	0.60	0.70	0.40
12	0.60	0.45	0.30	0.45	0.40	0.30	0.50
13	0.70	0.35	0.10	0.40	0.60	0.30	0.50
14	0.70	0.55	0.20	0.45	0.40	0.50	0.60
15	0.70	0.45	0.30	0.35	0.50	0.70	0.40
16	0.80	0.45	0.10	0.40	0.40	0.70	0.60
17	0.80	0.35	0.20	0.45	0.50	0.30	0.40
18	0.80	0.55	0.30	0.35	0.60	0.50	0.50

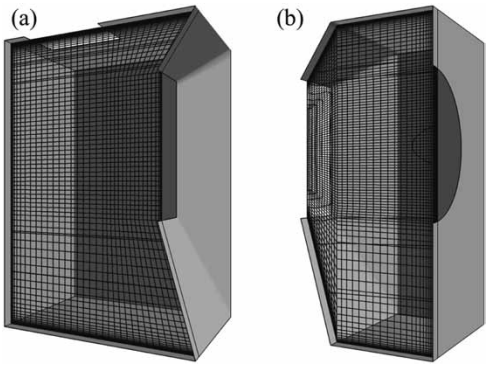

Fig. 5 Analytical models of intake ducts by CFD method
(a) Duct A, (b) Duct B

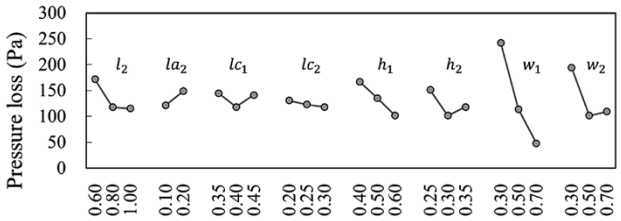

Fig. 6 Factor effect of Duct A

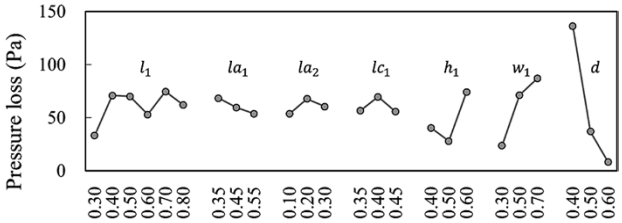

Fig. 7 Factor effect of Duct B

parameters related to the dimensions of the opening on the outflow side and is not capable of evaluating the changes in pressure loss due to the change in the shape of the outflow-side opening.

Hence, the modified equation takes into account not only the average flow velocity on the inflow side but also the average flow velocity on the outflow side. The modified equation consists of the weighted sum of the pressure loss value obtained by substituting the average flow velocity on the inflow side into Equations (1) through (3) and the pressure loss value obtained by substituting the average flow velocity on the outflow side into Equations (1) to (3). Moreover, the flow passage of Duct A has a bend of 90 degrees, and the length of the flow passage at the bent portion is considered to affect the pressure loss value. Hence, in addition to the area ratio of inflow side opening and outflow side opening, the length of the path connecting the center of the inflow side opening and the center of the outflow side opening was adopted as the weighting factor. For Duct B, the area ratio of inflow side opening and outflow side opening is assumed to contribute to the pressure loss value and was adopted as a weighting factor. Equations (4) to (9) are expressions predicting the pressure loss obtained. The prediction equation of pressure loss for Duct A is given by Equation (4):

$$\Delta P_A = \Delta P_{out} + \Delta P_{in} \frac{S_{in}}{S_{out}} \frac{(h_1/2)/h}{(l_2 - l_{c2} - l_{a2})/l_2} \quad \cdots\cdots (4)$$

wherein,

$$\Delta P_{in} = 1.808 m_A^{\frac{1}{8}} n_A^{\frac{1}{12}} \frac{\rho v_{in}^2}{2} \quad \cdots\cdots (5)$$

$$\Delta P_{out} = 1.808 m_A^{\frac{1}{8}} n_A^{\frac{1}{12}} \frac{\rho v_{out}^2}{2} \quad \cdots\cdots (6)$$

The prediction equation of pressure loss for Duct B is given by Equation (7).

$$\Delta P_B = \Delta P_{in} + \Delta P_{out} \left(\frac{S_{in}}{S_{out}} \right)^{0.2} - 20 \quad \cdots\cdots (7)$$

wherein,

$$\Delta P_{in} = \begin{cases} 0.324 m_B^{\frac{1}{8}} n_B^{\frac{1}{12}} \dfrac{\rho v_{in}^2}{2} & (\text{for } \theta = 0) \\ 2.021 m_B^{\frac{1}{8}} n_B^{\frac{1}{12}} (\tan\theta)^{\frac{1}{8}} \dfrac{\rho v_{in}^2}{2} & (\text{for } \theta \neq 0) \end{cases} \quad \cdots\cdots (8)$$

$$\Delta P_{out} = \begin{cases} 0.324 m_B^{\frac{1}{8}} n_B^{\frac{1}{12}} \dfrac{\rho v_{out}^2}{2} & (\text{for } \theta = 0) \\ 2.021 m_B^{\frac{1}{8}} n_B^{\frac{1}{12}} (\tan\theta)^{\frac{1}{8}} \dfrac{\rho v_{out}^2}{2} & (\text{for } \theta \neq 0) \end{cases} \quad \cdots\cdots (9)$$

Fig. 8 and **Fig. 9** show the pressure loss values obtained by CFD with the shapes shown in Table 1 and Table 2 (Calculation), the pressure loss values estimated by Yoshihara's equation, and the pressure loss values calculated from Equation (4) and Equation (7) (Modified equation). The Yoshihara's

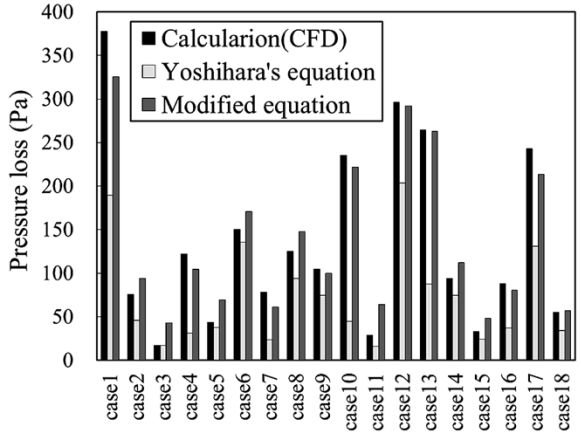

Fig. 8 Comparison of the estimated pressure loss in Duct A

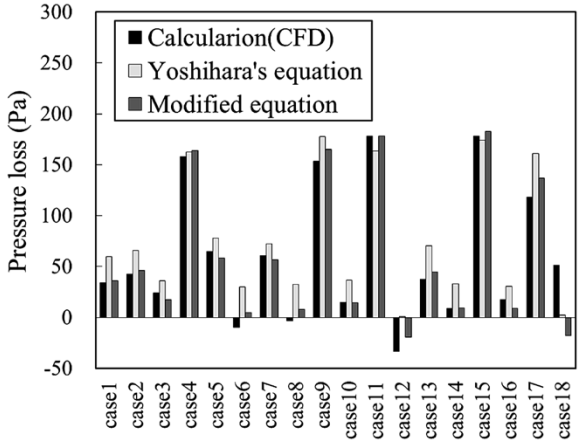

Fig. 9 Comparison of the estimated pressure loss in Duct B

equation departs from the CFD results, depending on the shape of the duct. This is probably because it is an estimation equation constructed on the basis of the experimental results when the inlet side inner diameter is fixed, and the pressure loss value cannot be accurately estimated for the duct shapes that are outside the applicable range. It is shown that Modified equation (4) and Modified equation (7) are the expressions that can reproduce the trends of the CFD results.

2.3 Mathematical modeling of noise attenuation performance

In the evaluation of Duct A's noise attenuation performance, a publicly known mathematical expression model is used, in which Duct A is regarded as a sound absorbing chamber. For the range of frequencies whose wavelengths are shorter than the dimensions of the duct, Equation (10) is used in accordance with the theory of indoor sound fields.[4] On the other hand, if the dimensions of the tube and the cavity are smaller than the wavelength of the sound and in the handling range of the plane wave, the attenuation amount of the insertion tube cavity is expressed by Equation (11).[5] Now, Duct B is regarded as an insertion tube cavity, and the noise attenuation performance is evaluated by Equation (11).

$$R_A = 10\log_{10}\left\{\frac{1}{S_{out}\left(\frac{\cos\theta}{2\pi d'}+\frac{1-\alpha}{\alpha S_w}\right)}\right\} \quad \cdots\cdots\cdots\cdots \quad (10)$$

$$R_B = 10\log_{10}\frac{1}{4}\left\{\left(1+\frac{S_c/S_{in}}{S_c/S_{out}}\right)\cos^2 kl_1 + \left(\frac{S_c}{S_{in}}+\frac{1}{S_c/S_{out}}\right)^2\sin^2 kl_1\right\} + 10\log_{10}\left(\frac{S_c/S_{out}}{S_c/S_{in}}\right) \quad \cdots\cdots\cdots \quad (11)$$

wherein,

- α : average indoor sound absorption coefficient
- S_{out}: outlet cross-sectional area
- S_c: cavity cross-sectional area
- S_{in}: inlet cross-sectional area
- S_W: duct interior surface area
- k: wavenumber
- d': distance between the inlet and outlet
- θ : the angle between the outlet opening plane and the direction connecting the inlet center and the outlet center.
- l_l: cavity length.

Because wavenumber k varies with frequency f_x, the noise attenuation performance of the duct expressed by Equations (10) and (11) has frequency dependence. Therefore, in order to reduce the OA value of the noise leaking out from the duct, it is necessary to assign frequency characteristics to the attenuation amount in accordance with the frequency characteristics of the noise source. Hence, in evaluating the noise attenuation performance of the muffler duct, the attenuation amounts $R_A(f_x)$ and $R_B(f_x)$ of the muffler duct were subtracted from the acoustic power level $L_{source}(f_x)$ of the sound source in each frequency band f_x to obtain a noise level $L(f_x)$, and the overall (OA) value, L_{OA}, was obtained by combining the noise levels of all the frequency bands. Equations (12) and (13) show the calculation formulae for the OA value, L_{OA}, and the noise level $L(f_x)$.

$$L_{OA} = 10\log_{10}\left(\sum 10^{\frac{L(f_x)}{10}}\right) \quad \cdots\cdots\cdots\cdots\cdots\cdots \quad (12)$$

$$L(f_x) = L_{source}(f_x) - \{R_A(f_x) + R_B(f_x)\} \quad \cdots\cdots\cdots\cdots \quad (13)$$

In this paper, the noise radiated from the engine and hydraulic pump of a hydraulic excavator was measured and used as the sound source.

2.4 Optimization of design parameter based on genetic algorithm

This paper describes a duct whose size has been randomly determined within the constraint range

of the design, in which the performance is evaluated using the ventilation resistance formula model and the noise attenuation performance formula model described above. The combinations of design variables determineded to have low ventilation resistance and high noise attenuation performance are kept as excellent combinations, while the combinations of design variables determined to have low performance are deleted. Repeating the above procedure weeds out any combinations other than those with low ventilation resistance and high noise attenuation performance, in the end, obtaining the combination of optimum design variables.

This problem is formulated as Equations (14):

$$\begin{aligned} &\textit{Minimize} \quad F_1 = \Delta P_A + \Delta P_B \\ &\textit{Minimize} \quad F_2 = L \\ &\textit{subject to} \quad G_1 > 0,\ G_2 > 0,\ \cdots,\ G_6 > 0 \end{aligned} \qquad \cdots\cdots (14)$$

The outer shape of the duct has a maximum value determined by the size of the machine body, and constraint conditions are generated for the design parameter representing the inner shape of the duct.

The constraint conditions, G_1 to G_6, are given by Equations (15).

$$\begin{aligned} G_1 &= l_{c1} - \frac{1}{2} h_1 \\ G_2 &= h - \left(l_{c1} + \frac{1}{2} h_1 \right) \\ G_3 &= l_{c2} - \frac{1}{2} h_2 \\ G_4 &= l_2 - \left(l_{a2} + l_{c2} + \frac{1}{2} h_2 \right) \\ G_5 &= h - \left(l_{a1} + \frac{1}{2} d \right) \\ G_6 &= l_{a1} - \frac{1}{2} d \end{aligned} \qquad \cdots\cdots (15)$$

When applied to GA, the constraint conditions G_1 to G_6 in Equations (14) were regarded as unconstrained optimization problems on the basis of the penalty function method.

Fig.10 shows the distribution of ventilation resistance and noise level of the initial population generated by initialization, while **Fig.11** is an example of a set of design solutions obtained by GA. The comparison of the initial population of the design solution with the distribution of the final generation clarifies that the optimization using GA weeds out the design solution with large ventilation resistance and noise level to obtain a favorable design solution for ventilation resistance and noise level. The Pareto optimal solutions shown in Fig.11 are ones in which an attempt to improve either the ventilation resistance or noise level deteriorates the other. The design solution is selected from these Pareto optimum solutions in consideration of the individual importance of ventilation resistance and noise level.

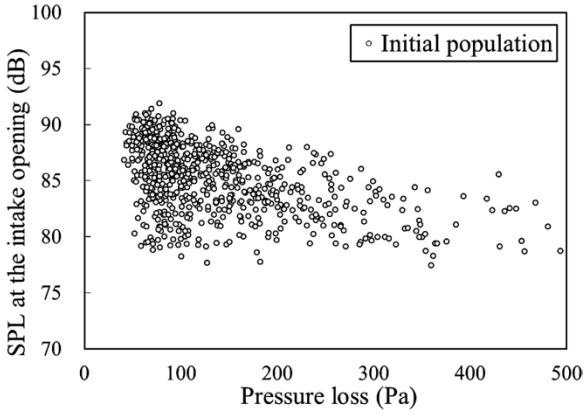

Fig.10 Distribution of the initial population

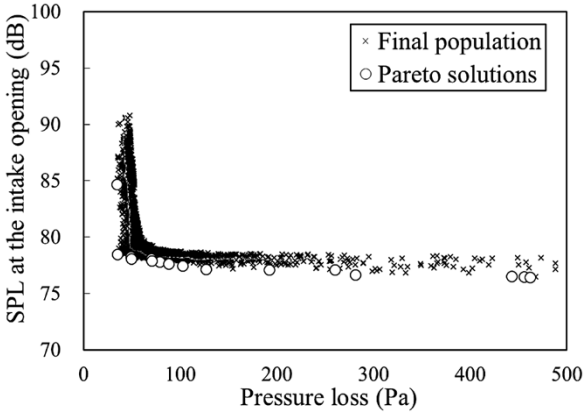

Fig.11 Distribution of the final population

3. Application to actual machines

The following describes the results of changing the intake duct layout, in which the change was made with reference to the ventilation resistance obtained by the optimization using GA and to the Pareto optimum solution of intake duct shape for reducing the noise level. In the case of the optimization using GA, the Pareto optimum solution is characterized by the enlarged opening area of the intake opening and the installation position of the dust filter being placed lower than in the conventional layout. This has been adopted as the shape of a new duct. Considering the placement of equipment to be installed inside the intake duct, the design parameters which are difficult to reproduce have been designed to take values as close as possible to the respective Pareto solutions. The acoustic power level in the intake opening of the new duct shape is shown in **Fig.12**. **Fig.13** shows the change rate of pressure loss before and after the change from conventional shape to new shape. As shown in Fig.12, the acoustic power level at

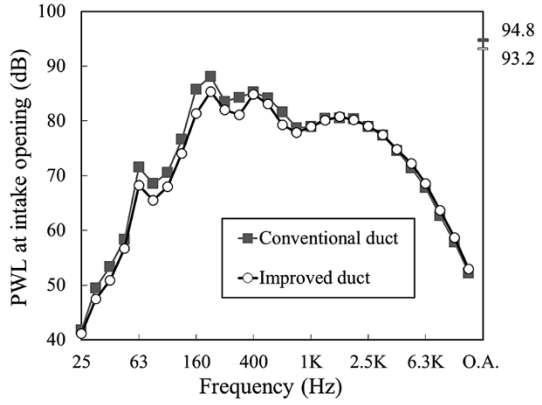

Fig.12 PWL at intake opening

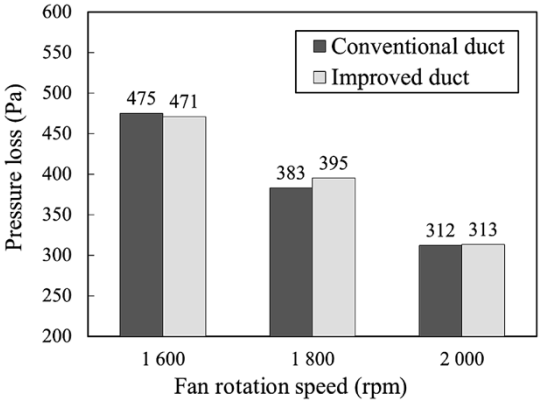

Fig.13 Change in pressure loss

the intake opening has decreased from 94.8 dB to 93.2 dB in terms of O.A. value, thanks to the shape change of the intake duct. As shown in Fig.13, the pressure loss deteriorates by approximately 3% at 1,800 rpm. However, it has achieved almost the same performance as the conventional shape.

As described above, the optimization technique according to this paper has made it possible to quickly implement the design of the duct to realize low noise while satisfying the cooling performance.

Conclusions

This paper has introduced a shape optimization technique using GA as a design technique to achieve both a low pressure loss and high noise attenuation performance of ducts. In this paper, the ventilation resistance and noise attenuation performance of the ducts subject to optimization are expressed by a mathematical model. Furthermore, the present model may be substituted with a response surface model based on the neural network or Kriging response surface method, enabling a solution to various design problems. We will strive to contribute to the development of machine products that meet the needs of society by applying this method.

References

1) H. Nakajima el al. *R&D Kobe Steel Engineering Reports*. 2012, Vol.62, No. 1, pp. 27-31.
2) M. Kubo et al. *Metaheuristics: A Programming Guide*, First edition, Kyoritsu Shuppan CO. LTD, 2009, pp. 61-62.
3) T. Yoshihara. *Ebara Engineering Review*. 1985, No. 130, pp.2-7.
4) H. Utsuno el al. *R&D Kobe Steel Engineering Reports*.1999, Vol.49, No.1, pp.56-59.
5) T. Katsuta el al. *AIJ Journal of Technology and Design*, 1959, 62, pp.79-85.